Structure and stability of Au rods on TiO_2(110) surfaces by first-principles calculations

Hongqing Shi,[1] Masanori Kohyama,[1,*] Shingo Tanaka,[1] and Seiji Takeda[2]
[1]*Research Institute for Ubiquitous Energy Devices, National Institute of Advanced Industrial Science and Technology (AIST), 1-8-31, Midorigaoka, Ikeda, Osaka 563-8577, Japan*
[2]*Department of Physics, Graduate School of Science, Osaka University, 1-1, Machikaneyama, Toyonaka, Osaka 560-0043, Japan*
(Received 20 July 2009; published 5 October 2009)

In order to examine atomic and electronic structures of the perimeter of Au-particle/TiO_2 systems related to the catalytic activity, we perform density-functional theory calculations of Au-rod/TiO_2(110) models with the relationship of Au(111)[0−11]‖TiO_2(110)[001] observed by electron microscope. We deal with models of different interface stoichiometry with various rigid-body translations. For the stoichiometric systems, stable configurations have Au-O bonds between edge-Au and bridging-O atoms at the perimeter. For the Ti-rich systems with bridging-O atoms removed under a Au rod, rather strong Au-Ti bonds with covalent nature are formed and appear at the perimeter as well as weak Au-O bonds. For the O-rich systems formed by digging a pit under a Au rod, quite strong Au-O bonds with significant Au 5*d*-O 2*p* hybridization and charge transfer like gold-oxides are formed and appear at the perimeter as well as rather weak Au-O bonds. About the relative stability among the systems with different stoichiometry, *ab initio* atomistic thermodynamics has shown that the O-rich Au/TiO_2 systems can be the most stable in usual atmosphere of the catalyst formation, indicating the importance of the perimeter of O-rich interfaces.

DOI: 10.1103/PhysRevB.80.155413 PACS number(s): 68.43.Bc, 68.47.Jn, 82.65.+r, 82.60.Qr

I. INTRODUCTION

In contrast to the long-held view that Au is catalytically inert, Haruta found that Au nanoparticles on metal oxides such as TiO_2 exhibit strong catalytic activity.[1] For example, Au/TiO_2 systems reveal unique catalytic activity for low-temperature CO oxidation and for epoxidation of propylene in a gas containing oxygen and hydrogen.[2–5] Extensive studies of Au/TiO_2 systems suggested a number of mechanisms of the catalytic activity such as quantum size effects of two-layer Au islands,[6] perimeter sites of Au-particle/TiO_2 systems,[7] abundance of low Au-Au coordination sites,[8] and charge transfer between Au and substrate.[9,10]

To elucidate the mechanism, it is essential to investigate the Au/TiO_2 interfacial interactions. Zhang *et al.*[11] studied the growth of Au films on rutile TiO_2(110) surfaces using low-energy ion scattering (LEIS) and x-ray photoelectron spectroscopy (XPS), and observed that evaporated Au initially grows quasi-two-dimensionally on stoichiometric surfaces without substantial chemical interactions between Au and TiO_2 substrate. Okazawa and co-workers[12,13] also analyzed the growth mode of Au particles on TiO_2(110) surfaces by using medium-energy ion scattering (MEIS) and photoelectron spectroscopy (PES), and found that three-dimensional island growth occurs at the initial stage for the reduced TiO_2(110) surface in contrast to the initial two-dimensional (2D) growth on the stoichiometric surface, indicating localized strong interactions between Au and the reduced TiO_2(110) substrate. About the electron microscopy observations, Akita *et al.*[14] observed preferred orientation relationships between a Au particle and TiO_2 support, where the Au(111) plane is parallel to the rutile TiO_2(110) plane or the anatase TiO_2(112) plane. Recently, they performed high-angle annular dark-field scanning transmission electron microscope (HAADF-STEM) observation of Au nanoparticles on rutile,[15] and found the preferential relationship of Au(111)[1−10]‖TiO_2(110)[001]. This should be caused by small lattice misfit along Au[1–10] and TiO_2[001] less than 3% experimentally. The HAADF-STEM image with clear atomic-column resolution of Au and Ti shows that the interlayer distance between the Au and Ti layers is 0.33 nm, while O atoms or columns cannot be detected, preventing determination of precise interface configurations or stoichiometry.

On the theoretical side, density-functional theory (DFT) calculations have been extensively applied to the atomic and electronic structures of Au/TiO_2(110) systems in last ten years. The full-potential linearized augmented plane-wave (FLAPW) calculation[16] predicted that the most stable Au-monolayer (1×1) adsorption site on the rutile TiO_2(110) surface is the on-top site above the fivefold Ti atom, Ti[5]. About the effects of defects or non-stoichiometry on the TiO_2 surface, Wahlsröm *et al.*[17] clarified that Au clusters are strongly bonded to a bridging-O vacancy on the rutile TiO_2(110) surface by scanning tunneling microscopy (STM) and *ab initio* pseudopotential calculations, indicating that bridging-O vacancies are the active nucleation sites for Au clusters, which is consistent with a lot of experimental observations.[13] Other DFT calculations[18–22] also showed that Au atoms or clusters are much more strongly bonded to O vacancies or reduced TiO_2 surfaces than to the stoichiometric surface.

Apart from the reduced or stoichiometric TiO_2 surfaces, O-rich or oxidized Au/TiO_2 systems may exist in practical catalysts, because usual Au/TiO_2 catalysts are chemically produced by the precipitation method followed by calcination in air, while the O-rich TiO_2 surface itself is not so easily formed. Okazaki *et al.*[18] first performed DFT calculations of Au-monolayer adsorption on an O-rich TiO_2(110) surface, and observed the formation of strong Au-O bonds with significant Au 5*d*-O 2*p* hybridization and substantial electron transfer from Au to O in contrast to the stoichiometric or Ti-rich systems. Wang and Hammer[23] examined the behavior of Au_7 clusters on an oxidized (alkaline) TiO_2(110)

surface with OH adsorption on Ti^5 sites by DFT calculations, and found the strong adhesion of the Au cluster onto the TiO_2 substrate with formation of cationic Au atoms. Such strong adhesion was also identified by STM.[24]

In the present study, we perform DFT calculations about the perimeter configurations of Au/rutile-TiO_2(110) systems. A lot of experiments indicate that the perimeter region is the key of the catalytic activity.[7] The bonding characters at the Au/TiO_2 interface mentioned above, such as termination species, interfacial charge transfer, namely, formation of cationic or anionic interfacial Au atoms, and interfacial orbital hybridization, should affect the chemical reactions via the exposure at the perimeter edge. In order to examine realistic configurations of the perimeter regions of Au/TiO_2 systems and their electronic or chemical states, we deal with probable Au-rod/TiO_2-substrate models with the relationship of $Au(111)[1-10]\|TiO_2(110)[001]$ observed in the recent HAADF-STEM observation.[15] For this alignment, we can utilize the coincident periodicity along Au[1–10] and TiO_2[001], which enables us to deal with rather large models, and we can make comparison with the observed images.

To examine various possibilities, we deal with the Au-rod/TiO_2 models of three types of interface stoichiometry, namely, stoichiometric, Ti-rich, and O-rich systems. For each type of stoichiometry, we introduce various rigid-body transitions (RBTs) between the Au rod and TiO_2 substrate. Then, we analyze Au-O and Au-Ti bonds at the interface and perimeter regions, and discuss the general features of the perimeter configurations. Previously, Au-rod/TiO_2 models were constructed and the chemical reaction associated with the perimeter region was examined by DFT calculations,[10] while only several configurations of stoichiometric and Ti-rich systems were dealt with. In the present study, O-rich interfaces are constructed by digging a pit beneath the Au rod so as to make direct contact between O atoms inside TiO_2 and the Au rod, in contrast to the removal of only bridging-O atoms under the Au rod for Ti-rich interfaces. This is due to the necessity of changing the interface plane in TiO_2 under the Au rod with other TiO_2 surface regions kept stoichiometric. This point is natural in comparison with recent HAADF-STEM images of Au/TiO_2 interfaces with a pit or step on the TiO_2 surface.[15] We make thermodynamic analysis of relative stability among the systems with different stoichiometry as a function of the oxygen chemical potential. This can clarify the effects of the atmosphere for the catalyst formation or catalytic reactions. For O-rich systems, even though O-rich oxide surfaces are not stable in any atmosphere, O-rich metal/oxide interfaces can possibly become stable under the O-rich atmosphere as shown for metal/alumina systems.[25]

In Sec. II, we explain the DFT total-energy scheme, the construction of Au-rod/TiO_2(110) models, and the *ab initio* atomistic thermodynamics approach. In Sec. III, results for the stoichiometric, Ti-rich, and O-rich Au-rod/TiO_2(110) systems are presented, and the thermodynamic stability is examined. The nature of interfacial Au-O and Au-Ti bonds and the features of perimeter configurations are discussed. In Sec. IV, we give a summary.

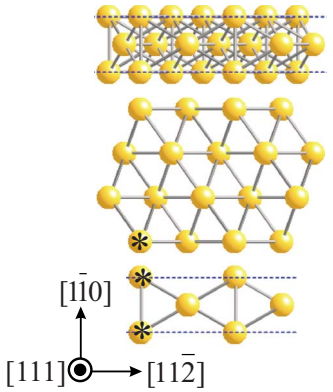

FIG. 1. (Color online) Top (upper) and side (middle) views of the initial atomic geometry of the Au rod. The top view of the Au atoms at the bottom layer of the rod is shown at the lower panel. The labeled atom Au^* is used to define an initial 2D-RBT between the Au rod and the TiO_2 substrate. The directions are those for the bulk Au in the top view.

II. THEORETICAL SCHEME

We perform DFT calculations using Vienna *ab initio* simulation package (VASP).[26–28] We employ the projector augmented wave (PAW) method[29,30] with the generalized-gradient approximation (GGA) for the exchange-correlation functional.[31] Valence wave functions are expanded in a plane-wave basis set with an energy cutoff of 29.4 Ry (400 eV). Electronic occupancies near the Fermi level are smeared by a Gaussian function with a temperature broadening of $k_BT=0.2$ eV (k_B is the Boltzmann constant) and the total energy is extrapolated to zero temperature. The PAW pseudopotentials are generated by taking scalar relativistic corrections into account. For a Ti pseudopotential constructed for four valence electrons as $3d^24s^2$, the lattice parameters of the rutile TiO_2 crystal are reproduced as $a=4.647$ Å and $c=2.968$ Å, which are consistent with the experimental ($a=4.587$ Å and $c=2.954$ Å)[32] and other theoretical values.[33] For the TiO_2(110) surface, the relaxed configuration is similar to the experimental[34,35] and other DFT results.[36] We have observed that the inclusion of Ti semicore $3p$ electrons as valence states does not induce significant effects on the TiO_2 bulk and (110) surface. For a Ti pseudopotential constructed so as to include $3p$ electrons as valence ($3p^63d^24s^2$), the calculated lattice parameters reveal negligible modifications as $a=4.643$ Å and $c=2.965$ Å, and the surface configuration has only minor changes, as observed in Ref. 33. Thus in order to reduce the computational efforts, we select the Ti pseudopotential for $3d^24s^2$. For Au, the lattice constant of fcc Au is reproduced as 4.175 Å, which is in good agreement with experimental (4.08 Å)[37] and other DFT values (4.18 Å).[38]

For the Au-rod/TiO_2(110) systems, the TiO_2(110) substrate is modeled by a four-layer slab using the calculated bulk lattice parameters. Each slab is separated by a vacuum region of 19.86 Å. A Au rod consisting of 18 Au atoms per period along the [1–10] axis is introduced on one side of the TiO_2 slab. As shown in Fig. 1, the Au rod is formed by (111) and (100) surfaces, which is a typical feature of a Au nanoparticle as observed by

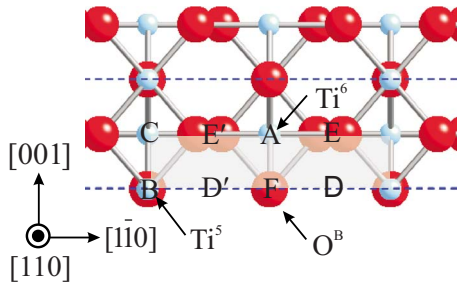

FIG. 2. (Color online) Top view of the irreducible region (gray) of the 2D-RBT between the Au rod and the $TiO_2(110)$ substrate. Eight symmetric points (A, B, C, D, D′, E, E′, F) are examined as initial configurations. The large and small spheres represent O and Ti atoms.

HAADF-STEM.[15] The ratio of each surface area depends on the relation of each surface energy. Namely, the shape is determined by the condition of the minimum energy for the surfaces within the constraints of the number of atoms. The present angles of the rod edge are rather similar to those in the HAADF-STEM images,[15] although the present rod has "minimal" size. The (3×1) $TiO_2(110)$ surface unit cell is adopted to deal with the Au rod, perimeter and TiO_2 surface regions. The Au rod is put on the $TiO_2(110)$ surface with the orientation relationship of Au(111)[1−10]∥TiO_2(110)[001], Au(111)[11−2]∥TiO_2(110)[1−10], and Au(111)[111]∥TiO_2(110)[110].[13] The period along [1–10] in the Au rod, which is 2.952 Å theoretically and 2.885 Å experimentally, has to be the same as the period along [001] in the rutile TiO_2, which is 2.968 Å theoretically and 2.954 Å (Ref. 32) experimentally. Thus, the initial Au rod is stretched along the [1–10] axis by 0.527%, and compressed by 0.2625% for both the [11–2] and [111] directions so as to keep of the atomic volume in Au.

We consider possible two-dimensional RBTs between the rod and substrate within the above crystallographic constraints. The 2D-RBT can be expressed as the 2D position of one specific Au atom of the rod in the (1×1) unit of the $TiO_2(110)$ surface, and the independent region of the 2D-RBT can be reduced into a half of the (1×1) unit as shown in Fig. 2, due to the mirror symmetry of both the rod and slab. For selected eight RBTs in Fig. 2, we construct initial configurations of the stoichiometric, Ti-rich and O-rich systems, by setting the Au rod on the stoichiometric surface, by removing bridging-O atoms under the Au rod, and by digging a pit under the Au rod so as to make Au-O direct contact, respectively.

The total cell volume is 1814 $Å^3$, containing 24 Ti, 48 O, and 18 Au atoms for the stoichiometric case. We use a $1\times12\times1$ Monkhorst-Pack k-point mesh,[39] resulting in 6 k-points in the irreducible Brillouin zone. The top three layers are relaxed until all the atomic forces are less than 0.01 eV/Å. This is consistent with recent published work.[40] The relaxed third layer also ensures accurate calculation for O-rich systems reported in this work, which are formed by digging a pit at the first layer on the $TiO_2(110)$ surface. The adhesive energy between the Au rod and the TiO_2 substrate is defined by

$$E_{ad} = E_{Au}^{rod} + E_{TiO_2}^{sub} - E_{Au/TiO_2}, \quad (1)$$

where E_{Au}^{rod}, $E_{TiO_2}^{sub}$, and E_{Au/TiO_2} represent the total energies of the free Au rod, the relaxed $TiO_2(110)$ substrate, and the Au-rod/$TiO_2(110)$ system, respectively.

The free energy of the Au-rod/$TiO_2(110)$ system depending on the stoichiometry and the environment atmosphere through the atomic chemical potentials is given by

$$F(T,p) = (G - N_{Au}\mu_{Au} - N_{Ti}\mu_{Ti} - N_O\mu_O)/A$$
$$= \{G - N_{Au}\mu_{Au} - N_{Ti}\mu_{TiO_2}^{bulk} - (N_O - 2N_{Ti})\mu_O]\}/A \quad (2)$$

within the constraints of $\mu_{Ti}+2\mu_O=\mu_{TiO_2}^{bulk}$. G is the Gibbs free energy of the Au/TiO_2 system. The total energy is the predominant term in G.[41] For pressures not exceeding about 100 atm, the contribution from the pV term in G is negligible, and we neglect vibrational contributions. A is the corresponding surface area. N_{Au}, N_{Ti}, N_O, μ_{Au}, μ_{Ti}, and μ_O are the numbers and atomic chemical potentials of each species, respectively. $\mu_{TiO_2}^{bulk}$ is the bulk-TiO_2 chemical potential per TiO_2 unit, approximated by the total energy of bulk TiO_2, $E_{TiO_2\text{-bulk}}^{total}$. μ_{Au} is also approximated by the total energy per atom of bulk fcc Au $E_{Au\text{-bulk}}^{total}$. Note that $F(T,p)$ contains the free energies of the Au-rod surface and the $TiO_2(110)$ surfaces on the both sides of the slab in addition to the free energy of the Au/TiO_2 interface. The T and p dependence is mainly given through $\mu_O=(1/2)\mu_{O_2}^{gas}$ as

$$\mu_O(T,p) = 1/2\left[E_{O_2}^{total} + \tilde{\mu}_{O_2}(T,p^0) + k_BT\ln\left(\frac{p_{O_2}}{p^0}\right)\right], \quad (3)$$

p_{O_2} is oxygen partial pressure of the environment, p^0 is the oxygen pressure in the standard state corresponding to atmospheric pressure, and $\tilde{\mu}_{O_2}(T,p^0)$ contains the contribution from rotations and vibrations of the molecule as well as the ideal-gas entropy at 1 atm.[41] For the O-rich limit, $\mu_O=(1/2)E_{O_2}^{total}$, and for the O-poor limit, $\mu_O=1/2(E_{TiO_2\text{-bulk}}^{total}-E_{Ti\text{-bulk}}^{total})$, where $E_{O_2}^{total}$ and $E_{Ti\text{-bulk}}^{total}$ are the total energy of an O_2 molecule and the total energy per atom of bulk hcp Ti, respectively.

III. RESULTS AND DISCUSSION

A. Stoichiometric Au-rod/TiO_2(110) system

Relaxed structures of the stoichiometric Au-rod/$TiO_2(110)$ systems with different initial RBTs are presented in Fig. 3. There are two groups of relatively stable configurations: one contains sA and sE′, and the other contains sD, sF, and sD′. Within each group, all the structures seem to be relaxed into a similar atomic configuration, respectively, in spite of different initial RBTs. sA and sF are the most stable in each group, respectively, while the adhesive energies are not so large, as compared with Ti-rich or O-rich systems described below. This means that the interfacial interaction between the Au rod and the stoichiometric $TiO_2(110)$ surface is generally small as observed in previous experiments[11–13] and DFT results.[16–24]

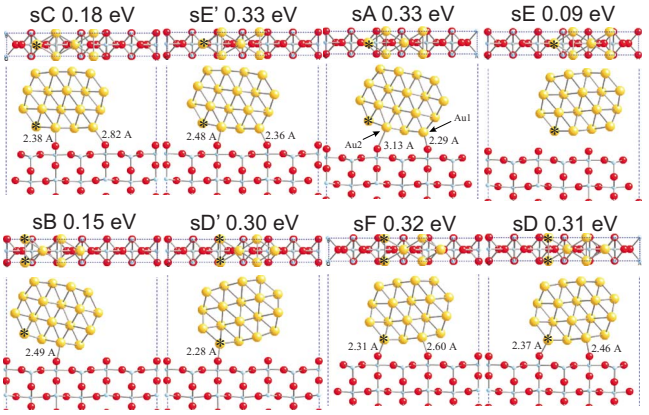

FIG. 3. (Color online) Top (upper) and side (lower) views of relaxed atomic geometries of the stoichiometric Au-rod/TiO_2(110) systems with eight types of initial 2D-RBTs in Fig. 2. The adhesive energy is given for each structure. Only the Au atoms at the bottom layer of the rod are shown in the top view. The labeled atom Au^* is used to define the initial 2D-RBT. The red, yellow, and small light blue spheres represent O, Au, and Ti atoms, respectively. The Au-O bonds are drawn with the bond-length value only when the length is less than 3.13 Å.

In each group, the stable structures are characterized by the presence of two kinds of Au-O bonds; one is a shorter bond between the edge-Au (Au^{ed}) and bridging-O (O^{br}) atoms, and the other is a longer bond between the bottom-Au (Au^{bt}) and O^{br} atoms. These Au-O bonds are formed for a Au atom just above a O^{br} atom as a one-by-one bond. The difference in the RBT as $(1/2)[001]TiO_2$ for the two groups of stable configurations causes different interfacial bond networks. In each group, there is a tendency that the structure with a shorter Au^{ed}-O^{br} bond such as sA and sF is more stable than those with a slightly longer Au^{ed}-O^{br} bond such as sE′ and sD. sD′ has indeed a very short Au^{ed}-O^{br} bond of 2.28 Å while the Au^{bt}-O^{br} bond seems to be too long. The short Au^{ed}-O^{br} bond seems to dominate the main part of the adhesion for the stable interfaces. This also indicates the stronger reactivity of edge-Au atoms than usual bottom-Au atoms in a Au rod, due to more reduced numbers of neighbors.

Detailed features of the Au-O bonds are analyzed for sA by the charge density redistribution and the projected density of states (PDOSs). The charge transfer at the Au^{ed}-O^{br} (Au1-O1) bond is much more than that at the Au^{bt}-O^{br} (Au2-O2) bond in Fig. 4. In Fig. 5, the PDOSs at the Au^{ed}-O^{br} (Au1-O1) bond reveal substantial Au-O orbital hybridization. The shape of the Au-5*d* DOS reveal changes compared to that in the free Au rod, and the shape of the O-2*p* DOS is significantly changed. The nonbonding O-2*p* peak at the free TiO_2 surface is greatly decreased and pushed down by the hybridization with the Au states. On the other hand, the PDOSs of the Au^{bt}-O^{br} (Au2-O2) bond reveal no remarkable changes for the Au-5*d* and O-2*p* DOSs from those in the free surfaces.

However, it can be said that the present Au-O bonds in the stoichiometric systems are not so strong as those observed in the O-rich interfaces described later. This "weakness" is caused by the following two points. First, the reactivity of

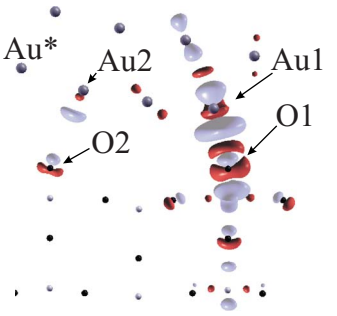

FIG. 4. (Color online) Charge density redistribution $n^{\Delta}(\mathbf{r})$ (Ref. 42) for the stoichiometric Au-rod/TiO_2 system, sA. The red isosurfaces indicate an increase in the electron density, and the light blue isosurfaces represent a depletion, compared to the superposition of the charges of the separated systems. The value of the isospheres is $\pm 1.2 \times 10^{-2}$ e/Å^3. The large gray, small light gray, and dark spheres represent Au, Ti, and O atoms.

the O^{br} atom on the TiO_2(110) surface is not so significant. The O^{br} atom loses one distant neighboring Ti atom, compared with the three neighboring Ti atoms in the bulk. For this point, the O^{br} atom may have some reactivity, while this O atom is firmly bonded to the two back Ti atoms without any gap states or any excess holes or electrons. Second, Au is usually less reactive than other metals, while edge-Au atoms with less coordination have enhanced reactivity.

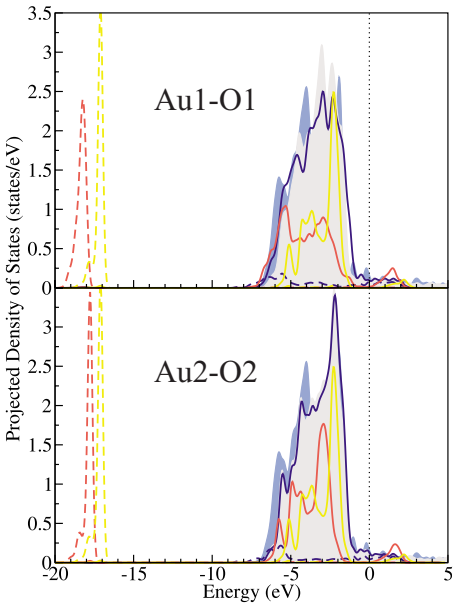

FIG. 5. (Color online) PDOSs of the stoichiometric Au-rod/TiO_2 system, sA. Upper and lower panels are for the Au1-O1 and Au2-O2 bonds, corresponding to the Au^{ed}-O^{br} and Au^{bt}-O^{br} bonds, respectively. The solid and dashed blue lines represent the Au-5*d* and 6*s* states, respectively. The light gray and light blue backgrounds denote the Au-5*d* states for the corresponding Au atom in the free relaxed Au rod and for the bulk Au, respectively. The solid and dashed red lines indicate the O-2*p* and 2*s* states, respectively, and the solid and dashed yellow lines indicate the O-2*p* and 2*s* states at the O^{br} atom on the relaxed stoichiometric TiO_2(110) surface. The Fermi energy is indicated by the vertical dotted line.

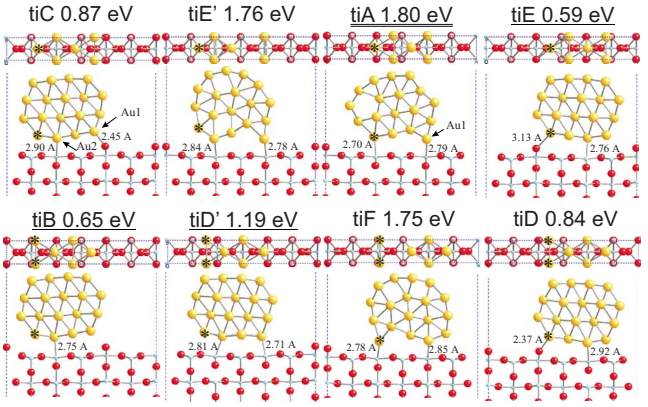

FIG. 6. (Color online) Top (upper) and side (lower) views of relaxed atomic geometries of the Ti-rich Au-rod/TiO_2(110) systems with eight types of initial 2D-RBTs in Fig. 2. The adhesive energy is given for each structure. Only the Au atoms at the bottom layer of the rod are shown in the top view. The labeled atom Au^* is used to define the initial 2D-RBT. The red, yellow, and small light blue spheres represent O, Au, and Ti atoms. The Au-Ti^4 bonds are drawn with the bond-length value only when the length is less than 3.00 Å, and the Au-O^{br} bonds are drawn with the bond-length value only when the length is less than 3.13 Å. Structures with a single underline at the title contain on-top Au-Ti^4 bonds, and those without a underline at the title contain bridging Au-Ti^4 bonds, while the structure with a double underline at the title, namely, tiA, contains both kinds of Au-Ti^4 bonds.

The average interlayer distance between the bottom Au layer and the Ti layer for the relatively stable configurations such as sE′, sA, sD, sF, and sD′ is about 0.38 nm, which is larger than the experimental value of 0.33 nm.[15] The present inclining of the rod is associated with the short width of the rod. If the width of the rod is much longer, the inclining should become much smaller, while this should result in smaller averaged adhesive energy per area due to the reduced ratio of edge-Au atoms against usual bottom-Au atoms.

About the perimeter configuration, there are two types of typical structures. One is a rather open structure with Au-rod edge atoms and a TiO_2 surface exposed, and the other is that characterized by the Au^{ed}-O^{br} bonds. For the former type of structure, there should also exist O^{br} atoms nearby. Thus for the perimeter configurations of the stoichiometric systems, the combination between the reactive edge-Au atoms and the O^{br} atoms at the open structures or at the Au^{ed}-O^{br} bonds might be involved in catalytic reactions via bond switching.

B. Ti-rich Au-rod/TiO_2(110) system

Relaxed configurations of the Ti-rich Au-rod/TiO_2(110) systems with different initial RBTs are presented in Fig. 6. After removing O^{br} atoms under a Au rod, fourfold Ti atoms (Ti^4) are generated, and direct Au-Ti^4 bonds are formed. There are two types of Au-Ti^4 bond configurations. One is an on-top one-by-one Au-Ti bond where a Au atom is located just above a Ti^4 atom. The other is a bridging two-by-two Au-Ti bond where an Au atom is located at the bridging site contacting with two Ti^4 atoms, forming a zigzag Ti-Au-Ti bond along the TiO_2[001] axis. The number of removed O^{br} atoms depends on the RBT along the TiO_2[1−10] direction. One O^{br} atom is removed per (3×1) unit cell for tiB, tiD, tiC, and tiE, and two O^{br} atoms are removed for tiD′, tiF, tiE′, and tiA. For each pair such as tiB and tiC with the same RBT along the TiO_2[1−10] direction, the different RBT along the TiO_2[001] direction results in the formation of different types of Au-Ti bonds.

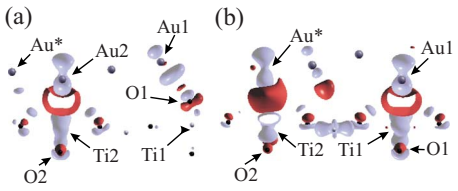

FIG. 7. (Color online) Charge density redistribution for the Ti-rich Au-rod/TiO_2 systems, (a) tiC and (b) tiA in Fig. 6. The red isosurfaces indicate an increase in the electron density, and the light blue isosurfaces represent a depletion, compared to the superposition of the charges of the separate systems. The value of the isospheres is $\pm 2.2\times10^{-2}$ e/Å^3. The large gray, small light gray, and dark spheres represent Au, Ti, and O atoms.

On the adhesive energies, it seems that the bridging Au-Ti^4 bonds are more beneficial to the adhesion than the on-top Au-Ti^4 bonds, and the larger density of removed O atoms results in the larger adhesive energy. For the group of tiB, tiC, tiD, and tiE, stable configurations with larger adhesive energies such as tiC and tiD contain the bridging Au-Ti^4 bonds as well as the Au^{ed}-O^{br} bonds similar to those in the stoichiometric systems. For the group of tiD′, tiE′, tiF, and tiA with much larger adhesive energies, structures with the bridging Au-Ti^4 bonds such as tiE′ and tiF are indeed stable, while the most stable tiA contains both the bridging and on-top Au-Ti^4 bonds. A high density of the bridging Au-Ti^4 bonds induces serious structural deformation of the Au rod in tiE′, tiF, and tiA in contrast to tiD′ containing only on-top Au-Ti^4 bonds. Such structural deformation may be caused by the fact that the distance between the defective Ti^4 sites along the TiO_2[1−10] direction does not coincide with the arrangement of Au atoms in the rod, while the small width of the present rod may also enhance the deformation. In any case, the adhesion between the Au rod and the TiO_2 substrate is greatly enhanced by the presence of O vacancies in contrast to the stoichiometric systems, as observed in previous DFT results.[17–22]

The Au-Ti interlayer distances of the present Ti-rich systems are generally smaller than the observed one (0.33 nm).[15] For example, the value of tiC is 0.291 nm. Of course, the present width of the rod is rather small as compared with the observed particle size, and there is a possibility that the observed interface corresponds to a partially reduced interface instead of a completely reduced one.

Detailed features of the Au-Ti bonds are analyzed for tiC and tiA by the charge density redistribution and the PDOSs. In Fig. 7, apparent charge density increases between the Au and Ti atoms indicate covalent nature of the Au-Ti^4 bonds. This feature is consistent with previous DFT results.[18–22] For the bridging bonds (Au2-Ti2 in tiC and Au1-Ti1 in tiA), there are two increased charge robes around each atom, compared with the on-top bond (Au^*-Ti2 in tiA). The charge

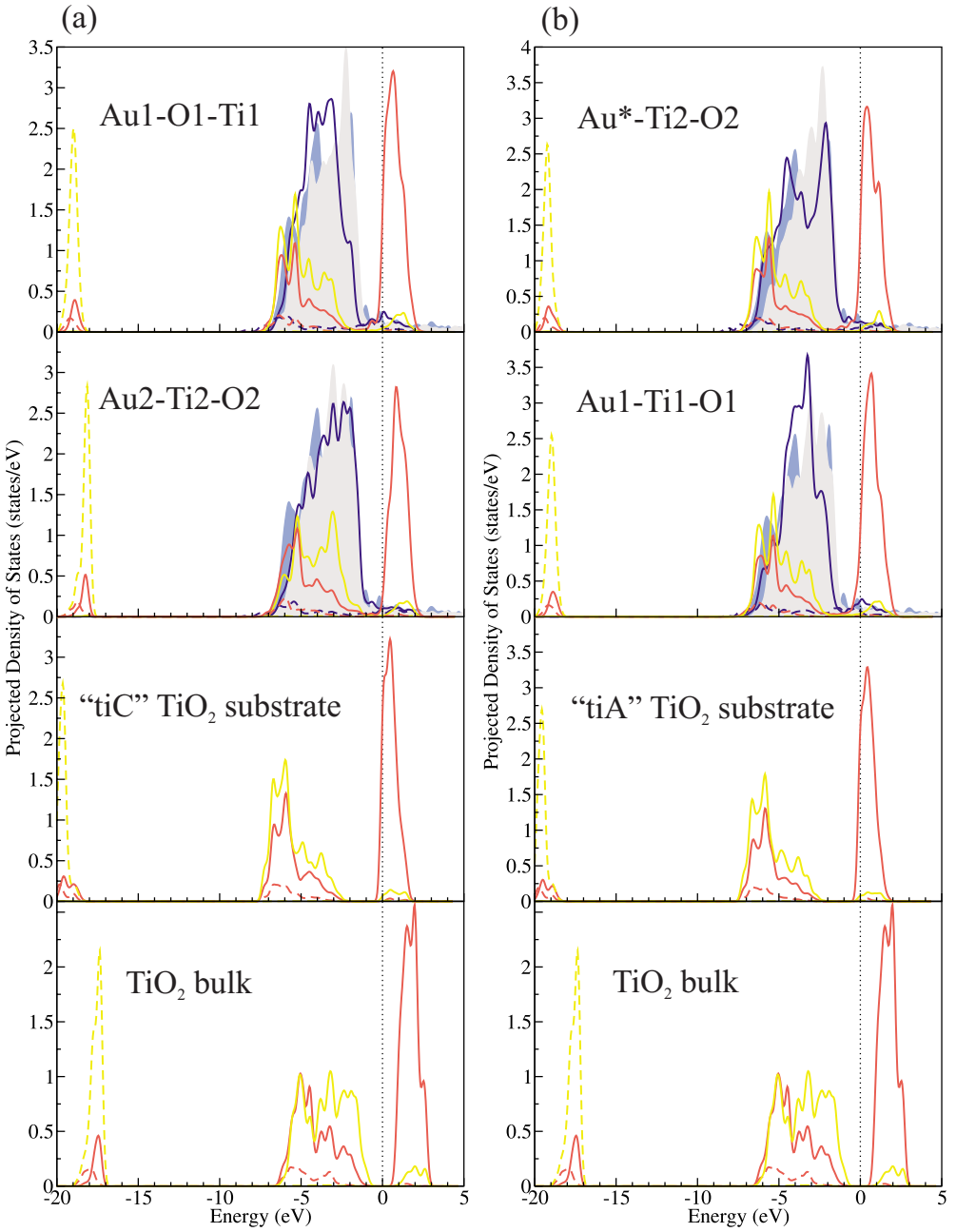

FIG. 8. (Color online) PDOSs of the Ti-rich Au-rod/TiO_2(110) systems, tiC (a) and tiA (b). The top and second panels show the PDOSs at the Au-Ti and Au-O bonds shown in Fig. 7. The third panels show the PDOSs at the Ti^4 and back-bonded O atoms of the relaxed configuration of each TiO_2 substrate, and the bottom panels show the PDOSs of the bulk TiO_2. The solid and dashed lines in blue, red, and yellow represent the Au-5*d* and 6*s*, Ti-3*d* and 4*s*, and O-2*p* and 2*s* states, respectively. The light gray and light blue backgrounds denote the Au-5*d* states for the corresponding Au atoms in the free relaxed Au rod and for the bulk Au, respectively. The Fermi energy is indicated by the vertical dotted line.

increase value at the Au-Ti bond itself is larger for the on-top bond than for the bridging bond, due to the shorter bond length. In tiC, there also exists slight charge transfer from Au to O at the Au^{ed}-O^{br} (Au1-O1) bond similarly to those in the stoichiometric systems.

In Fig. 8, the change of the Au-5*d* DOS is remarkable at the on-top Au-Ti^4 bond, namely, at the Au^*-Ti2 bond in tiA, where the 5*d* DOS has a peculiar split shape. For the bridging bonds such as Au2-Ti2 in tiC and Au1-Ti1 in tiA, the Au-5*d* DOSs are less changed from those of the free Au rod. This should be caused by the longer Au-Ti bond length of the bridging bond than that of the on-top bond. However, for all the Au-Ti bonds, we can see the increases in the occupied PDOSs of Au 5*d* and Ti 3*d* in the energy region below the Fermi level, as compared with the PDOSs of the defected TiO_2 substrate. For the Au1-O1 bond in tiC, there exist features of Au-O hybridization as observed for the Au^{ed}-O^{br} bond in the stoichiometric system.

The possible perimeter configurations for the Ti-rich systems can be sorted as the following kinds: on-top Au-Ti^4

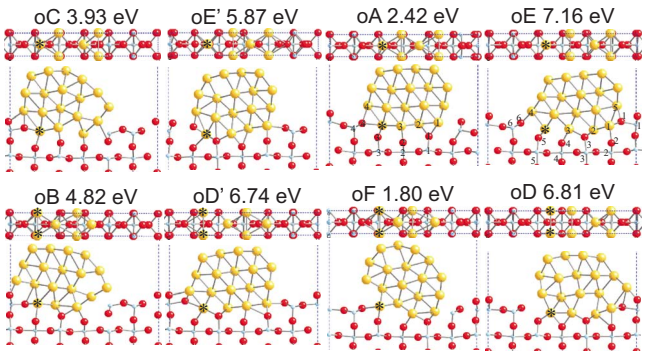

FIG. 9. (Color online) Top (upper) and side (lower) views of relaxed atomic geometries of the O-rich Au-rod/TiO_2(110) systems with eight types of initial 2D-RBTs in Fig. 2. The adhesive energy is given for each structure. Only the Au atoms at the bottom layer of the rod are shown in the top view. The labeled atom Au^* is used to define the initial 2D-RBT. The Au-O bonds are drawn only when the length is less than 3.13 Å. The red, yellow, and small light blue spheres represent O, Au, and Ti atoms.

bonds at the Au-rod edge (tiD′ and tiA), bridging Au-Ti^4 bonds at the Au-rod edge (tiE′, tiF, and tiA), Au^{ed}-O^{br} bonds (tiC, tiD, and tiE), and open configurations consisting of the edge-Au atoms and the bare TiO_2 surface. The Au atoms at the Au-Ti bonds may have different chemical properties for the interaction with molecules. The Au^{ed}-O^{br} bonds and open configurations seem to be common to the stoichiometric systems, and might be involved in catalytic reactions via bond switching between the Au and O^{br} atoms.

C. O-rich Au-rod/TiO_2(110) system

Relaxed configurations of the O-rich Au-rod/TiO_2(110) systems with different initial RBTs are presented in Fig. 9. The numbers of removed Ti and O atoms at the interface depend on the RBT along the $TiO_2[1-10]$ axis. For oB, oC, oF, and oA, three Ti and five O atoms are removed per (3×1) cell, resulting in one excess O atom. Within these models, the total energies of oF and oA are much lower than those of oB and oC, and oA is the most stable. The larger adhesive energies of oB and oC do not mean the stability relative to oF and oA, due to the difference in the total energy of the TiO_2 substrate as the origin of the adhesive energy. The TiO_2 substrate of oB and oC has a much higher total energy than that of oF and oA due to the difference in the position of a pit. For oA, the structural distortion at the Au rod seems to be the smallest within the four structures. For oD′, oE′, oD, and oE, four Ti, and five O atoms are removed per (3×1) cell, resulting in three excess O atoms. The total energies of oD and oE are much lower than those of oD′ and oE′, and oE is the most stable. For oE, the structural distortion at the Au rod also seems to be the smallest within the four structures.

As compared with the observed HAADF-STEM images,[15] the calculated configurations are much more disordered at the interface. For relatively ordered configurations, the averaged Au-Ti interlayer distances at the interface are 0.363 nm for oA and 0.316 nm for oE, which are rather comparable to the observed value, 0.33 nm.[15] However, the interface planes are located in a pit compared to the usual TiO_2(110) surface plane, and the observed structure with the interlayer distance of 0.33 nm does not show such features. Thus we cannot conclude that the observed configurations are O-rich, while such pits or steps are occasionally observed.[15]

In oA in Fig. 9, there exist several types of Au-O bonds. The first type is an on-top one-by-one Au-O bond between an edge or bottom-Au atom and a O^{br} atom with two back O-Ti bonds, as observed in the stoichiometric and Ti-rich systems. Au3-O2 (2.24 A) and Au4-O4 (2.48 A) bonds belong to this type, while O4 atom with two back O-Ti bonds forms an additional one-by-one bond as Au^*-O4 (2.74 Å). The second type is a bridging two-by-two Au-O bond, where each Au and O atoms contact with two O and two Au atoms, respectively, and an O atom is supported by only one O-Ti back bond. Au^*-O3 (2.27 Å) and Au2-O1 (2.58 Å) bonds belong to this type, while O1 forms Au1-O1 one-by-one bond (2.26 Å) additionally. Thus O1 is located on the center of a triangle of Au atoms, and thus Au2-O1-Au1 can be also regarded as the third type of Au-O bonds.

In oE in Fig. 9, there also exist similar types of Au-O bonds. First, Au4-O6 (2.17 Å), Au3-O4 (2.17 Å), and Au1-O2 (2.37 Å) bonds are the on-top one-by-one Au-O bonds supported by two back O-Ti bonds, while Au3 and Au1 are also involved in other Au-O bonds. Second, Au^*-O5 (2.10 Å), Au2-O3 (2.14 Å), and Au1-O1 (2.21 Å) bonds are the bridging two-by-two Au-O bonds supported by only one O-Ti back bond, while one-by-one bonds are additionally formed at O3 and O1 as Au3-O3 (2.34 Å) and Au5-O1 (2.21 Å). Thus, Au2-O3-Au3 and Au1-O1-Au5 can be regarded as the third type of bonds between a Au triangle and an O atom.

The PDOSs for oE are shown in Fig. 10. For the bridging Au-O bonds such as Au^*-O5, Au2-O3, and Au1-O1, the PDOSs reveal significant Au 5*d*-O 2*p* hybridization, where the Au-5*d* DOSs are remarkably widened by the generation of peaks near the bottom and top of the 5*d* band with the overlap of the peaks of the broadened O-2*p* DOS, corresponding to the formation of Au-O bonding and antibonding states. Some peaks at the top of the 5*d* band are empty, indicating stabilization of the covalent Au-O bonds. Note that the O atoms associated with the bridging Au-O bonds have only one O-Ti back bond, resulting in remarkable changes in the 2*p* DOS, in contrast to the other O atoms with two O-Ti back bonds revealing no such remarkable changes. The PDOSs of Au3-O3 and Au5-O1 also reflect the features of Au 5*d*-O 2*p* hybridization due to the third type of bonds as Au2-O3-Au3 and Au1-O1-Au5, although the changes in the PDOSs at Au3 and Au5 are less significant. For the on-top Au-O bonds such as Au4-O6, Au3-O4, and Au1-O2, the Au 5*d*-O 2*p* hybridization is less significant, where the Au-5*d* and O-2*p* DOSs remain less changed from those in a Au rod or TiO_2 surfaces, except for the PDOS of Au1.

In Fig. 11, the charge density redistribution for oE reveals strong ionic characters of the Au-O bonds. Electrons are transferred from Au to O atoms at each interface Au-O bond, making the interfacial Au atoms partially cationic. This kind of electron redistribution is consistent with DFT results of Au-atom adsorption on an O-rich TiO_2(110) surface,[18] and

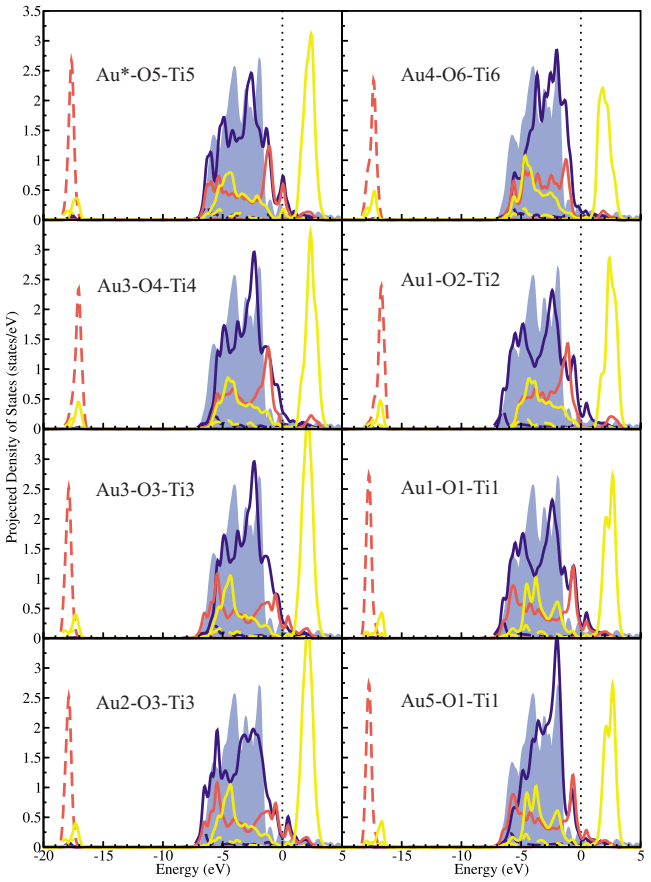

FIG. 10. (Color online) PDOSs of the O-rich Au-rod/TiO_2(110) system oE in Fig. 9. The solid and dashed lines in blue, red, and yellow represent the Au-5*d* and 6*s*, O-2*p* and 2*s*, and Ti-3*d* and 4*s* states, respectively. The light blue background represents the Au-5d states in the bulk Au. The labels of the Au, O, and Ti atoms are defined in Fig. 9. The Fermi energy is indicated by the vertical dotted line.

STM and DFT results of Au-cluster adsorption on an O-rich TiO_2(110) surface.[23,24] In Fig. 11, it is interesting that charge transfer at the on-top Au-O bond (Au4-O6, Au3-O4, and Au1-O2) is less than that at the bridging Au-O bonds (Au^*-O5, Au2-O3, and Au1-O1). This feature in addition to the feature of hybridization indicates that the on-top Au-O bond is much weaker than the bridging Au-O bond in both

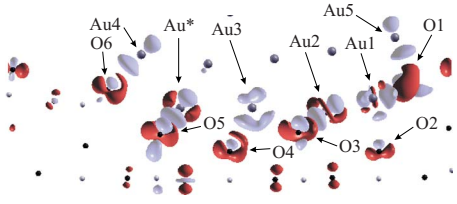

FIG. 11. (Color online) Charge density redistribution for the O-rich Au-rod/TiO_2 system oE in Fig. 9. The red isosurfaces indicate an increase in the electron density, and the light blue isosurfaces represent a depletion, compared to the superposition of the charges of the separate systems. The value of the isospheres is $\pm 5.0 \times 10^{-2}$ e/Å^3. The large gray, small light gray, and dark spheres represent Au, Ti, and O atoms.

the ionic and covalent viewpoints. This weakness of the on-top Au-O bonds is similar to the Au^{ed}-O^{br} or Au^{bt}-O^{br} bonds observed in the stoichiometric and Ti-rich systems. The bridging Au-O bonds or the third type of bonds between the Au triangle and O atoms are typical of the O-rich systems, revealing strong ionic and covalent characters. In such bonds, O atoms are supported by only one O-Ti back bond, which should cause such strong Au-O interactions.

The present Au-O bonds have similar features to those in gold-oxides such as Au_2O_3 and oxidized Au surfaces obtained by DFT calculations.[42–44] In the Au_2O_3 crystal, each Au atom is bonded to four O atoms in a AuO_4 unit, and O atoms are bonded to two or three Au atoms. The calculated Au-O bond lengths range from 1.99 Å to 2.11 Å,[43] and the average is 2.06 Å. The PDOSs show significant Au 5*d*-O 2*p* hybridization, where the new peaks common to the Au-5*d* and O-2*p* bands are generated near the bottom and top of the *d* band with the highest peaks unoccupied by a small band gap. The favorable oxidized Au(110)-surface structure contains similar AuO_4 units, where the shortest Au-O bond length is 2.03 Å.[44] In the favorable oxidized Au(100)-surface structure, the bond lengths between the O atom and its three neighbors are 2.11, 2.11 and 2.20 Å.[44] The PDOSs for these two oxidized Au surfaces reveal significant Au 5*d*-O 2*p* hybridization similar to those in Au_2O_3. The charge redistributions for the Au_2O_3 crystal and the oxidized surfaces reveal remarkable charge transfer from Au to O at each Au-O bond. For the present O-rich Au-rod/TiO_2 systems, the bridging Au-O bonds and the third type of Au-O bonds between the Au triangle and O atom have covalent and ionic characters, similar to the Au-O bonds in gold-oxides and oxidized Au surfaces. However, the Au-O bond lengths in the O-rich Au-rod/TiO_2 systems are slightly larger than those in gold-oxides and oxidized Au surfaces, and thus the degree of Au-O orbital hybridization seems to be reduced. This should be caused by the presence of back O-Ti bonds.

About the perimeter configuration of the O-rich systems, there exist the on-top Au-O bonds, the bridging Au-O bonds and the third type of bonds at the perimeter edge, where partially cationic Au atoms with strong hybridization with O orbitals should have quite different chemical properties. There also exist rather open structures at the perimeter with O^{br} atoms nearby, as well as rather weak on-top Au-O bonds at the perimeter. These sites also may be involved in the catalytic reaction via bond switching between the Au atom and the O^{br} atom.

D. Thermodynamic analysis

Figure 12 shows the results of *ab initio* thermodynamic analysis, revealing relative stability among various Au-rod/TiO_2 systems as a function of the O chemical potential. For the Ti-rich systems, the higher the density of O vacancies, the steeper the gradient of the lines of the free energies. For $\Delta\mu_O$ less than −3.26 eV, tiA becomes more stable than tiC. For the O-rich systems, the higher the density of excess O atoms, the steeper the gradient of the lines of the free energies. For $\Delta\mu_O$ larger than −0.92 eV, oE becomes more stable than oA. For the relation among the three types

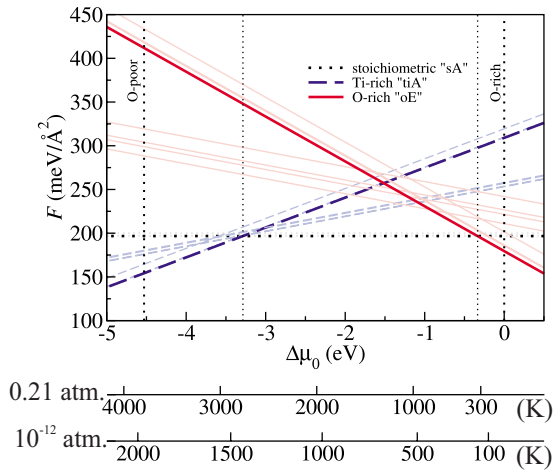

FIG. 12. (Color online) Free energies of the Au-rod/TiO_2(110) systems with various interface stoichiometry as a function of the O chemical potential. The free energy for the most stable stoichiometric system, sA, is given by the dotted horizontal line. The blue dashed lines with positive gradients represent the free energies of the Ti-rich systems. Two kinds of positive gradients reflect two kinds of stoichiometry for the Ti-rich systems. The thick dashed line represents the free energy of tiA, which becomes the most stable for the Ti-rich (O-poor) atmosphere. The red solid lines with negative gradients represent the free energies of the O-rich systems. Two kinds of negative gradients reflect two kinds of stoichiometry for the O-rich systems. The thick solid line represents the free energy of oE, which becomes the most stable for the O-rich atmosphere. In the horizontal axis, $\Delta\mu_O$ is defined as $\mu_O-(1/2)E_{O_2}^{total}$. Using Eq. (3), the corresponding temperatures are given for two selected oxygen partial pressures, $p_{O_2}=10^{-12}$ atm (7.6×10^{-9} Torr) as ultrahigh vacuum and $p_{O_2}=0.21$ atm in air of 1 atm. The most left and right vertical lines indicate the O-poor limit and O-rich limit.

of interface stoichiometry, the Ti-rich configuration, tiA, is the most stable for $\Delta\mu_O<-3.29$ eV. For the range of $\Delta\mu_O$ from −3.29 to −0.33 eV, the stoichiometric configuration, sA, is the most stable. Then for $\Delta\mu_O>-0.33$ eV, the O-rich one, oE, is the most stable. If we express the range of $\Delta\mu_O$ by temperatures, tiA is the most stable for $T>1433$ K in UHV and for $T>2760$ K in air ($p_{O_2}=0.21$ atm). oE is the most stable for $T<170$ K in UHV and for $T<328$ K in air. And sA is the most stable for the range of T from 170 to 1433 K in UHV, and for the range of T from 328 to 2760 K in air.

It is interesting that the O-rich configuration oE is the most stable in the atmosphere of the catalytic reaction such as low-temperature CO oxidation. On the atmosphere of the production of Au/TiO_2 catalysts, O-rich configurations can exist for the catalysts formed by the precipitation method followed by calcination in air, while samples formed by the vacuum deposition[15] should mainly contain stoichiometric or Ti-rich configurations. In any case, the present results indicate the importance of examining the perimeter configurations of O-rich Au/TiO_2 interfaces to elucidate the catalytic mechanism.

IV. SUMMARY

We have examined the Au-rod/TiO_2(110) systems using the DFT in order to investigate the perimeter configurations of Au-particle/TiO_2 systems related to the catalytic activity. We have dealt with various configurations of stoichiometric, Ti-rich, and O-rich interfaces with various 2D-RBTs. We have observed several kinds of typical Au-O and Au-Ti bonds, which should be generally contained in Au/TiO_2 interfaces with different stoichiometry and RBTs. The stoichiometric interfaces are characterized by Au^{ed}-O^{br} and Au^{bt}-O^{br} bonds. The former is stronger with substantial orbital hybridization and charge transfer due to the enhanced reactivity of edge-Au atoms, while both kinds of Au-O bonds are rather weak due to the two firm back O-Ti bonds for the O^{br} atom, compared to strong Au-O bonds in the O-rich interfaces. Similar Au^{ed}-O^{br} bonds are also formed at the perimeter of the Ti-rich interfaces. The O-rich interfaces contain much stronger Au-O bonds such as bridging two-by-two Au-O bonds and Au-O bonds between a Au triangle and an O atom, with significant Au 5*d*-O 2*p* hybridization and charge transfer from Au to O, similarly to those in gold-oxides and oxidized Au surfaces. These strong Au-O bonds are characterized by only one back O-Ti bonds. The O-rich interfaces also contain rather weak Au-O bonds with two back O-Ti bonds similar to the Au^{ed}-O^{br} or Au^{bt}-O^{br} bonds. The Ti-rich interfaces contain two types of Au-Ti^4 bonds with covalent nature; on-top one-by-one bonds and bridging two-by-two bonds, and the latter type is more beneficial to the adhesion.

On the other hand, the perimeter configurations obtained from the present calculations have the following features. First, for the Ti-rich interfaces, the Au-Ti bridging or on-top bonds can be exposed at the perimeter edge, which should have different chemical properties due to different charged and hybridized states. Second, for the O-rich interfaces, the strong Au-O bridging bonds or bonds between a Au triangle and an O atom can be also exposed at the perimeter edge, which should have also different chemical properties due to different charged and hybridized states. Third, the Au^{ed}-O^{br} bonds or similar on-top Au-O bonds can be exposed at the perimeter edge for all the stoichiometric, Ti-rich and O-rich interfaces, as well as rather open configurations consisting of edge-Au atoms and a TiO_2 surface with O^{br} atoms nearby. At these Au^{ed}-O bonds or open structures, the bond switching between the Au^{ed} and O^{br} atoms may be involved in the catalytic reactions. In this way, the behavior of molecules on the present typical perimeter-edge configurations should be examined in the near future in order to elucidate the mechanism of the catalytic activity. And the thermodynamic analysis has indicated the importance of examination of the O-rich systems.

ACKNOWLEDGMENTS

We thank Tomoki Akita and Masatake Haruta for fruitful discussions. This study was supported by Grant-in-Aid for Specially Promoted Research (Grant No. 19001005), and the Japan Society for the Promotion of Science Research (JSPS).

*m-kohyama@aist.go.jp

[1] M. Haruta, Catal. Today **36**, 153 (1997).
[2] T. Kobayashi, M. Haruta, H. Sano, and M. Nakane, Sens. Actuators **13**, 339 (1988).
[3] S. Lin and M. A. Vannice, Catal. Lett. **10**, 47 (1991).
[4] S. Lin, M. Bollinger, and M. A. Vannice, Catal. Lett. **17**, 245 (1993).
[5] T. Hayashi, K. Tanaka, and M. Haruta, J. Catal. **178**, 566 (1998).
[6] M. Valden, X. Lai, and D. W. Goodman, Science **281**, 1647 (1998).
[7] M. Haruta, Chem. Rec. **3**, 75 (2003).
[8] M. Mavrikakis, P. Stoltze, and J. K. Norskov, Catal. Lett. **64**, 101 (2000).
[9] Z. P. Liu, X. Q. Gong, J. Kohanoff, C. Sanchez, and P. Hu, Phys. Rev. Lett. **91**, 266102 (2003).
[10] L. M. Molina, M. D. Rasmussen, and B. Hammer, J. Chem. Phys. **120**, 7673 (2004).
[11] L. Zhang, R. Persaud, and T. E. Madey, Phys. Rev. B **56**, 10549 (1997).
[12] T. Okazawa, M. Fujiwara, T. Nishimura, T. Akita, M. Kohyama, and Y. Kido, Surf. Sci. **600**, 1331 (2006).
[13] T. Okazawa, M. Kohyama, and Y. Kido, Surf. Sci. **600**, 4430 (2006).
[14] T. Akita, K. Tanaka, S. Tsubota, and M. Haruta, J. Electron Microsc. **49**, 657 (2000).
[15] T. Akita, K. Tanaka, M. Kohyama, and M. Haruta, Surf. Interface Anal. **40**, 1760 (2008).
[16] Z. Yang, R. Wu, and D. W. Goodman, Phys. Rev. B **61**, 14066 (2000).
[17] E. Wahlström, N. Lopez, R. Schaub, P. Thostrup, A. Ronnau, C. Afirch, E. Lægsgaard, J. K. Norskov, and F. Besenbacher, Phys. Rev. Lett. **90**, 026101 (2003).
[18] K. Okazaki, Y. Morikawa, S. Tanaka, K. Tanaka, and M. Kohyama, Phys. Rev. B **69**, 235404 (2004).
[19] Y. Wang and G. S. Hwang, Surf. Sci. **542**, 72 (2003).
[20] A. Vijay, G. Mills, and H. Metiu, J. Chem. Phys. **118**, 6536 (2003).
[21] N. Lopez, J. K. Norskov, T. V. W. Janssens, A. Carlsson, A. Puig-Molina, B. S. Clausen, and J.-D. Grunwaldt, J. Catal. **225**, 86 (2004).
[22] T. Pabisiak and A. Kiejna, Phys. Rev. B **79**, 085411 (2009).
[23] J. G. Wang and B. Hammer, Phys. Rev. Lett. **97**, 136107 (2006).
[24] D. Matthey, J. G. Wang, S. Wendt, J. Matthiesen, R. Schaub, E. Lægsgaard, B. Hammer, and F. Besenbacher, Science **315**, 1692 (2007).
[25] W. Zhang, J. R. Smith, and A. G. Evans, Acta Mater. **50**, 3803 (2002).
[26] G. Kresse and J. Hafner, Phys. Rev. B **47**, 558 (1993); **49**, 14251 (1994).
[27] G. Kresse and J. Furthmüller, Comput. Mater. Sci. **6**, 15 (1996).
[28] G. Kresse and J. Furthmüller, Phys. Rev. B **54**, 11169 (1996).
[29] G. Kresse and D. Joubert, Phys. Rev. B **59**, 1758 (1999).
[30] P. E. Blöchl, Phys. Rev. B **50**, 17953 (1994).
[31] J. P. Perdew, J. A. Chevary, S. H. Vosko, K. A. Jackson, M. R. Pederson, D. J. Singh, and C. Fiolhais, Phys. Rev. B **46**, 6671 (1992).
[32] J. K. Burdett, T. Hughbanks, G. J. Miller, J. W. Richardson, Jr., and J. V. Smith, J. Am. Chem. Soc. **109**, 3639 (1987).
[33] H. Perron, C. Domain, J. Roques, R. Drot, E. simoni, and H. Catalette, Theor. Chem. Acc. **117**, 565 (2007).
[34] R. Lindsay, A. Wander, A. Ernst, B. Montanari, G. Thornton, and N. M. Harrison, Phys. Rev. Lett. **94**, 246102 (2005).
[35] G. Charlton, P. B. Howes, C. L. Nicklin, P. Steadman, J. S. G. Taylor, C. A. Muryn, S. P. Harte, J. Mercer, R. McGrath, D. Norman, T. S. Turner, and G. Thornton, Phys. Rev. Lett. **78**, 495 (1997).
[36] S. J. Thompson and S. P. Lewis, Phys. Rev. B **73**, 073403 (2006).
[37] C. Kittel, *Introduction to Solid State Physics* (Wiley, New York, 1996).
[38] S. D. Miller and J. R. Kitchin, Surf. Sci. **603**, 794 (2009).
[39] H. J. Monkhorst and J. D. Pack, Phys. Rev. B **13**, 5188 (1976).
[40] S. Fernandez, A. Markovits, and C. Minot, J. Phys. Chem. C **112**, 14010 (2008).
[41] K. Reuter and M. Scheffler, Phys. Rev. B **65**, 035406 (2001).
[42] H. Q. Shi and C. Stampfl, Phys. Rev. B **76**, 075327 (2007).
[43] H. Q. Shi, R. Asahi, and C. Stampfl, Phys. Rev. B **75**, 205125 (2007).
[44] H. Q. Shi and C. Stampfl, Phys. Rev. B **77**, 094127 (2008).